International Journal of Fluid Machinery and Systems
Vol. 4, No. 3, July-September 2011

DOI: 10.5293/IJFMS.2011.4.3.324
ISSN (Online): 1882-9554

Original Paper

Phase Resonance in a Centrifugal Compressor

Yumeto Nishiyama[1], Takayuki Suzuki[2], Koichi Yonezawa[1], Hiroshi Tanaka[3], Peter Doerfler[4], and Yoshinobu Tsujimoto[1]

[1] Department of Mechanical Science and Bioengineering,
Graduate School of Engineering Science, Osaka University
1-3 Machikaneyama, Toyonaka, Osaka 560-8531, Japan,
[2]Department of Mechanical Engineering, Kobe-City college of Technology
8-3, Gakuenhigashimachi, Kobeshi-kitaku, 651-2194, Japan,
[3]Toshiba Corporation (Retired)
[4]R&D Department, Andritz Hydro Ltd, Zurich, Switzerland

Abstract

Phase resonance in a centrifugal compressor was experimentally observed and simulated with a commercial CFD code. It was found that pressure fluctuation at the volute outlet becomes the maximum when the rotational speed of the modes caused by the rotor-stator interaction agrees with the sound velocity. A simple one-dimensional theory is presented to explain the phase resonance in turbomachinery.

Keywords: Phase resonance, Rotor-stator interaction, Centrifugal compressor, Volute, Numerical analysis

1. Introduction

The present study is motivated by the vibration of power house structure of a pumped storage power plant [1]. It was found in the field tests that the amplitude of vibration is increased when the runner speed is increased to the level in which the rotational speed of the pressure fluctuation mode caused by the rotor-stator interaction agrees with the sound propagation velocity in the volute.

This phenomenon is known as “phase resonance” and a theoretical model has been proposed by Den Hartog[2] and Chen [3] and examined in detail by Doerfler [4]. In Den Hartog and Chen’s theoretical model, a resonance condition at the inlet or at the narrow end of the volute occurs when the disturbance from each guide vane channel caused by the interaction with the runner blades has the same phase at the respective end of the volute. Thus, in Chen’s model, the rotor (runner)-stator(guide vane) interaction and the wave propagation in the volute are treated simultaneously. Unlike in the present study, the reflection of waves at the cutwater is neglected. In [4], like Chen[3], assuming a discrete source at each guide vane channel, the resulting intensity at the volute ends is estimated by a trigonometric summation formula, thus quantifying the resonance risk also in such cases where the Chen criterion is not exactly fulfilled. An example in a large pump has been reported by Makey et al.[5] in which the onset condition is examined based on Den Hartog’s methods. The possibility of phase resonance in Grand Coulee pump[6] is suggested.

One of the present authors, Hiroshi Tanaka, found that the resonance condition by Chen agrees, under several assumptions, with the condition that the rotational speed of the interaction mode becomes sonic speed. The present work is intended to study the phase resonance in more detail, using a compressor for vacuum cleaner. Phase resonance is treated by separating into two steps, the rotor-stator interaction and the acoustic wave generation/propagation in the volute. Total reflection of waves travelling towards the narrow end of the volute is assumed. Accordingly, the predicted resonance behavior differs from the older Chen/Doerfler model.

2. Rotor-stator interaction

The rotor-stator interaction has been treated by Tyler & Sofrin [7] for the study of axial flow compressor noise. We consider the interaction of equally spaced *R* rotor blades with equally spaced *S* stator blades as shown in Fig.1. The pressure pattern caused by the stator number *s=1* with *R* rotor blades is represented by

Received May 20 2011; accepted for publication June 24 2011: Review conducted by Prof. Yang-jun Zhang. (Paper number O11011C)
Corresponding author: Yoshinobu Tsujimoto, Professor, tujimoto@me.es.osaka-u.ac.jp

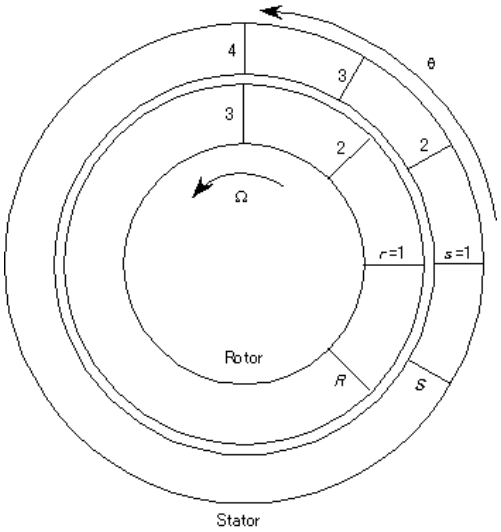

Fig. 1 Rotor-stator interaction model

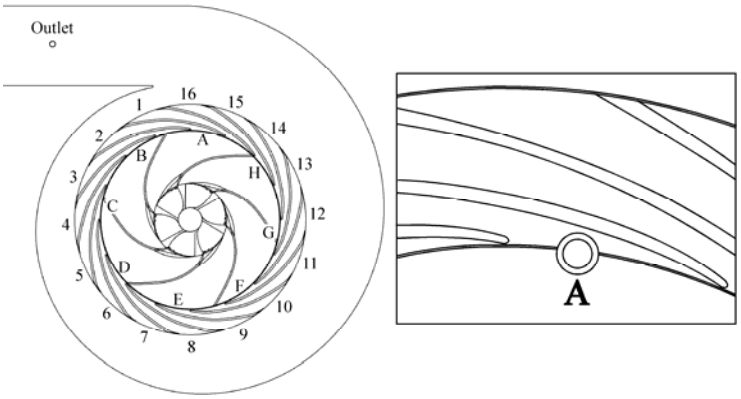

Fig. 2 Test compressor

Table 1 Specifications of rotor, stator and volute

Rotor	**Number of blades, *R***	**6**
	Outer Diameter, D_T[m]	**0.09**
Stator	**Number of blades, *S***	**16**
	Outer Diameter[m]	**0.121**
Volute mean diameter, Dv[m]		**0.14**

$$p_{m,n}^{s=1}(\theta,t) = a_{m,n} \cdot \cos(m\theta - nR\Omega t) \tag{1}$$

where, Ω is the angular velocity of the rotor, *m* and *n* are the order of harmonics in θ and *t*.

By considering the location of another stator *s*=*q* and the time for the rotor blade to move to the stator *s*=*q*, and by summing up the contribution of each stator blade, we obtain the following expression:

$$\begin{aligned} p_{m,n}(\theta,t) &= \sum_{q=1}^{S} p_{m,n}^{s=q}(\theta,t) \\ &= a_{m,n}\sum_{q=1}^{S}\cos\left[m(\theta-\frac{2\pi}{S}(q-1)) - nR\Omega(t-\frac{2\pi}{S\Omega}(q-1))\right] \\ &= \begin{cases} S\cdot a_{m,n}\cos m(\theta-\dfrac{nR}{m}\Omega t), & m = nR+kS \\ 0, & m \neq nR+kS \end{cases} \end{aligned} \tag{2}$$

where, *k* is an arbitrary integer number. This equation shows that the pressure pattern can rotate much faster than the rotor when $|nR/m| >> 1$.

3. Experimental facility and numerical simulation

Figure 2 shows the compressor used for the experiment. The rotor and stator were taken out from a vacuum cleaner. The stator blades were continued to a return channel but only the diffuser part was used in the present experiment after machining. The volute and downstream pipe were newly manufactured for the present study. The specifications of the compressor components are shown in Table 1.

The experimental facility is shown in Fig.3. The pressure fluctuations were measured by pressure transducers flush mounted at the stator inlet and the volute outlet.

Numerical simulations were made by using a commercial software ANSYS CFX-12.0. SST model was used as the turbulence

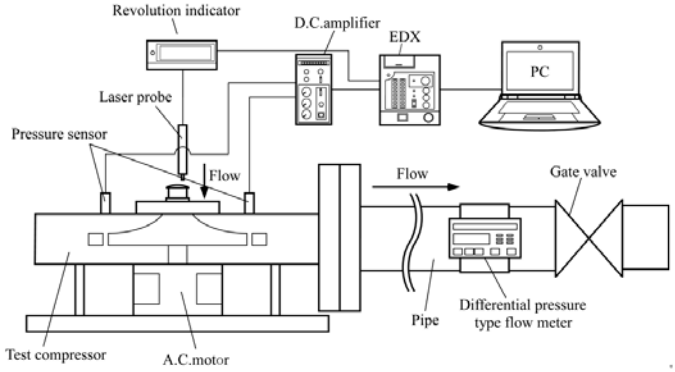

Fig. 3 Experimental facility

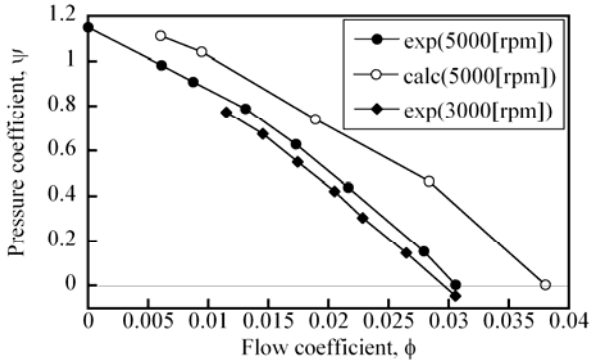

Fig. 4 Steady performance

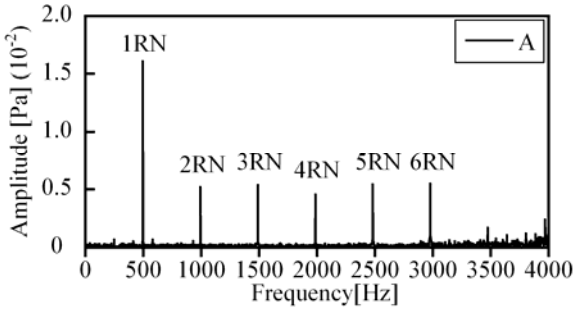

(a) Spectrum at stator inlet A (Exp.)

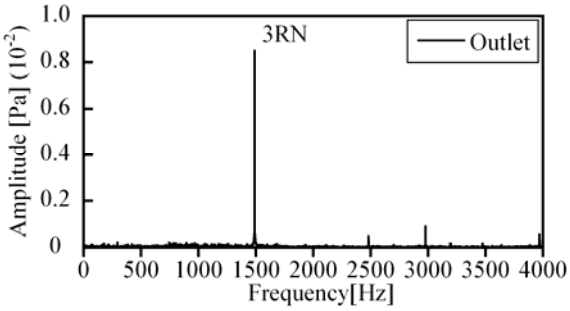

(b) Spectrum at volute outlet (Exp.)

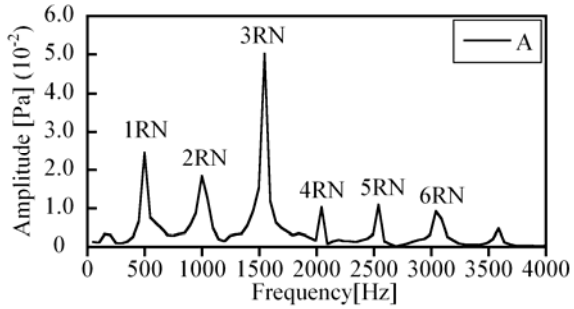

(c) Spectrum at stator inlet A (CFD)

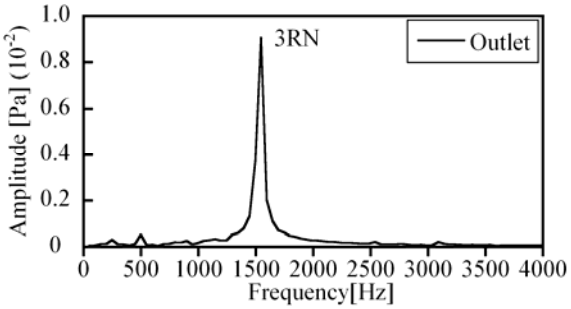

(d) Spectrum at volute outlet (CFD)

Fig. 5 Spectra of pressure fluctuation at stator inlet and volute outlet at N=5,000rpm (Exp.: ϕ=0.031, CFD: ϕ=0.038)

model. About 2,000,000 cells were used with 300 time steps per rotor rotation. Although the experimental facility does not have an inlet pipe of the compressor, the inlet pipe is added in the computational domain in order to enhance the numerical stability.

4. Experimental and numerical results

4.1 Steady performance

Figure 4 shows the steady performance curve obtained by experiment and CFD, at 5,000rpm. The flow coefficient is defined as $\phi = Q/(U_T D_T^2)$, and the pressure coefficient by $\psi = (P_{out} - P_{in})/(0.5\rho U_T^2)$ using the volumetric flow rate Q, rotor tip speed U_T, rotor outer diameter D_T, the fluid density at the inlet ρ, the inlet total pressure p_{in} , and the outlet static pressure p_{out}. Measurements were made at 3,000rpm-10,000rpm. The head was slightly smaller below 5,000rpm but no significant difference was found over 5,000rpm.

4.2 Pressure fluctuation at the stator inlet and the volute outlet

The spectra of the pressure fluctuation at the stator inlet A and the volute outlet (see Fig.2) for N=5,000rpm are shown in Fig.5. The comparison between the experimental and the numerical results are carried out with the results at the no load flow rate: ϕ=0.031 for the experiment and ϕ=0.038 for the simulation. All the harmonics of the blade passing frequency *RN* can be observed at the stator inlet, while only *3RN* can be found at the volute outlet. The agreement between experiment and CFD is not good, perhaps caused by the inaccuracy of the geometry and insufficient geometrical and temporal resolutions. Similar spectra were obtained for other flow rates and other rotational speed larger than 4,000rpm.

Figure 6 shows the effect of rotational speed and flow rate on the amplitude of pressure fluctuation at the volute outlet, from experiments. The pressure fluctuation is normalized with $0.5\rho U_T^2$. The numerical results with ϕ=0.038 corresponding to the no load operation conditions at the experiment with ϕ=0.031 are also shown in the figure. The agreement with measurement is rather surprising, if we consider the disagreement of the spectra at the stator inlet. The amplitude becomes the maximum at 5,000 rpm at all flow rate. The amplitude is the largest at the largest flow rate of ϕ=0.031. Since the fundamental characteristics does not depend on the flow rate, the results will be shown only for ϕ=0.031 for the experiment and ϕ=0.038 for the simulation.

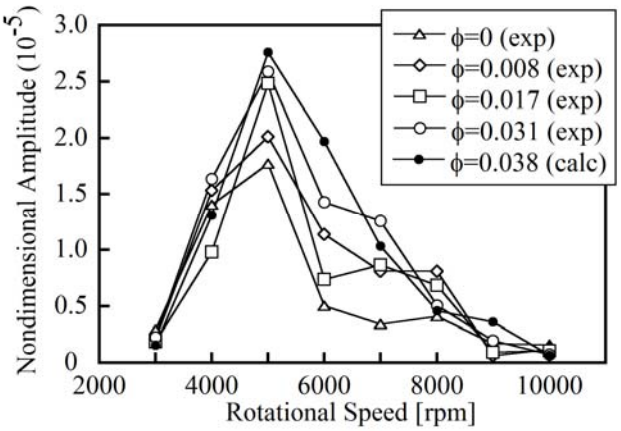

Fig. 6 Amplitude of pressure fluctuation at volute outlet

Now we consider why only the third harmonic *3RN* of the blade passing frequency is found at the volute exit. Equation (2) shows that the pressure fluctuation mode with $p_{m,n}(\theta,t) = S \cdot a_{m,n} \cos(\theta - \frac{nR}{m}\Omega t)$ occurs when $m = nR+kS$. For the present case with $R=6$ and $S=16$, we have a case with $2=3 \times 6 - 1 \times 16$, i.e., $m=2$, $n=3$, and $k=-1$. In order to confirm that the mode with $m=2$ is occurring, the phase difference of the pressure fluctuation component with *3RN* was measured at the stator inlet A-H in Fig.2. It was found that the phase difference between A and C is about 180 degrees and is around 0 degree (actually 0-33 degrees) between A and E. This confirms that a mode with $m=2$ is rotating around the rotor. Equation (2) also shows that the angular velocity of the mode is $\frac{n}{m}R\Omega = \frac{3}{2}6\Omega = 9\Omega$. The tangential velocity of this mode at the mean radius of the volute, 0.07m at the speed of 5,000rpm where the pressure fluctuation at the volute exit becomes maximum is calculated to be $0.07 \times 9 \times 2\pi \times 5000/60=330$ m/s, which is close to the sound velocity of 340m/s. The difference can be caused by the choice of the mean radius of the volute. However, for simplicity, discussions will be made by assuming that the Mach number of the $m=2$ is $M=1$ at 5,000rpm. We should note that this velocity is not obtained at the rotor exit but at the mean radius of the volute. So, we can say that the pressure fluctuation at the volute becomes the largest when the tangential velocity of the interaction mode at the mean radius of the volute agrees with the sound velocity. Re-examination of the results in [1] shows that the amplitude of pressure fluctuation in the volute is slightly decreased when the runner speed is increased beyond the speed where the rotational speed of the interaction mode agrees with the sound velocity. This is consistent with the present result.

For axial flow compressors, Tyler and Sofrin [7] have shown that the pressure fluctuation decays axially when the pressure pattern at the compressor face rotates around the rotor at subsonic speed. This is caused by the cancelling of the pressure waves from different circumferential location and is called “duct cut-off” and used to reduce noise from axial flow fans. However, if the pressure pattern rotates at a supersonic speed, the axial decay does not occur and the pressure fluctuation is transmitted infinitely upstream/downstream. This condition is called “super-resonance”. With a single rotor, the pressure pattern rotates fixed to the rotor. So, a subsonic rotor does not emit noise caused by the steady pressure pattern around it. However, the interaction with inlet flow distortion or stator blades may cause a pressure pattern which is rotating much faster than the rotor and if the interaction pattern rotates with supersonic speed, the pressure fluctuation is transmitted to upstream/downstream infinity without decay.

Since the pressure fluctuation at the volute outlet becomes smaller when the tangential velocity of the rotating mode with $m=2$ and $n=3$ exceeds the sound velocity at 5,000rpm, the phenomenon observed here, the “phase resonance” is quite different from the “super-resonance” in axial flow compressors.

4.3 Rotating pressure pattern

Figure 7 shows the pressure pattern obtained by CFD. It is clear that the mode in the rotor corresponds to $m=2$ at all speeds, as expected. However, the modes in the volute corresponds to $m'=1,2,3$ and 4 at 3,000, 5,000, 7,000 and 10,000rpm, respectively. It was confirmed that the modes in the volute propagates in the direction of rotor rotation (towards the volute exit) with the sound velocity plus local fluid velocity for the cases of 5,000, 7,000 and 10,000rpm. However, at 3,000rpm, the pressure fluctuation in the volute is more like a standing wave. This will be discussed later.

5. One-dimensional theory of phase resonance

5.1 One-dimensional theory

The acoustic wave generation and propagation in the volute is modeled by those in a half infinite duct with the width b, as shown in Fig.8. The effect of steady flow is totally neglected. The volute tongue is assumed to be located at $x=0$, and the volute exit at $x=L$. The disturbance due to the rotor-stator interaction is represented by the introduction of the fluid into the duct with the velocity of $v(x, t)$ in the region $0<x<L$. Since the flow fluctuation from the stator causes the fluctuation of the momentum supply, it is represented by an external mass force f applied within $0<x<L$. Then, the continuity equation, the momentum equation and the isentropic equation results in the following non- homogeneous wave equation for the velocity disturbance $u(x,t)$ in the duct.

$$\frac{\partial^2 u}{\partial x^2} - \frac{1}{a^2}\frac{\partial^2 u}{\partial t^2} = \frac{1}{b}\frac{\partial v(x,t)}{\partial x} - \frac{1}{a^2}\frac{\partial f}{\partial t} \tag{3}$$

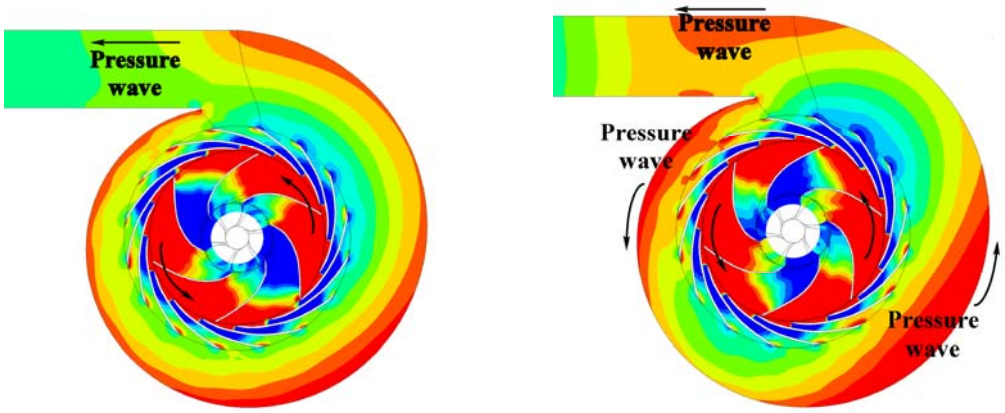

(a) *N=3,000rpm, M=0.6, m'=mM=1.2* (b) *N=5,000rpm, M=1.0, m'=mM=2.0*

(c) *N=7,000rpm, M=1.4, m'=mM=2.8* (d) *N=10,000rpm, M=2.0, m'=mM=4.0*

Fig. 7 Pressure pattern, from CFD (CFD: ϕ=0.038)

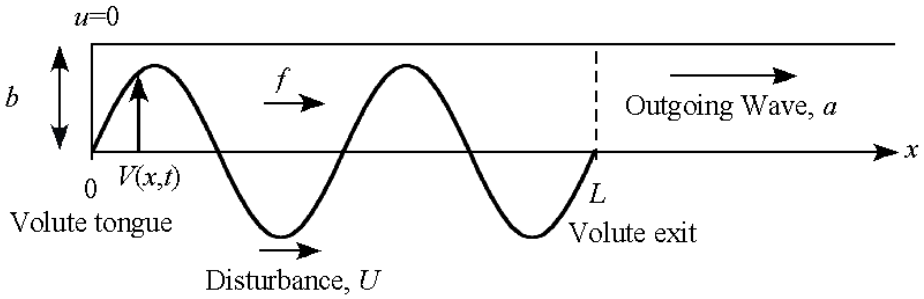

Fig. 8 One-dimensional acoustic model of the volute

Where, a is the sound velocity in the duct. In order to consider the disturbance caused by the interaction, we assume a sinusoidal disturbance:

$$\begin{cases} \dfrac{\partial^2 u}{\partial x^2} - \dfrac{1}{a^2}\dfrac{\partial^2 u}{\partial t^2} = -F\sin\left(\dfrac{2\pi m}{L}(x-Ut)\right) & (0<x<L) \\ \dfrac{\partial^2 u}{\partial x^2} - \dfrac{1}{a^2}\dfrac{\partial^2 u}{\partial t^2} = 0 & (L<x) \end{cases} \tag{4}$$

where, U is the phase velocity of the disturbance. The solution of this equation can be expressed as follows:

$$u = \left(\frac{L}{2\pi m}\right)^2 \frac{F}{1-M^2}\left[-e^{i\left(\frac{2\pi m}{L}U\left(t-\frac{x}{U}\right)\right)} + Ae^{i\left(\frac{2\pi m}{L}U\left(t-\frac{x}{a}\right)\right)} + Be^{i\left(\frac{2\pi m}{L}U\left(t+\frac{x}{a}\right)\right)}\right] \quad (0<x<L) \tag{5}$$

and

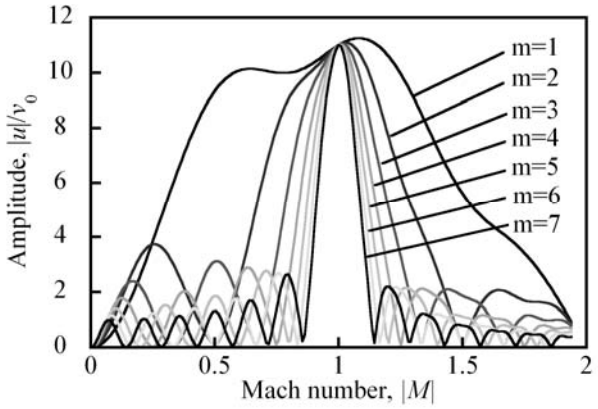

Fig. 9 Velocity disturbance at the volute exit $x=L$ caused by mass introduction for the case of $L/b=22$

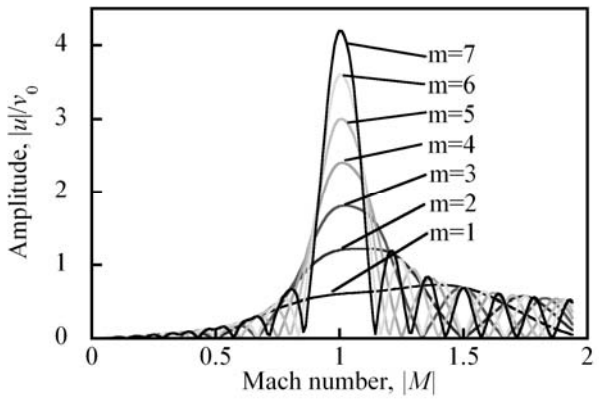

Fig. 10 Velocity disturbance at the volute exit $x=L$ caused by momentum introduction

$$u=\left(\frac{L}{2\pi m}\right)^2\frac{F}{1-M^2}Ce^{i\left(\frac{2\pi m}{L}U(t-\frac{x}{a})\right)} \qquad (x>L) \tag{6}$$

where, i is the imaginary unit (it is assumed that the imaginary part of complex quantities conveys the physical meaning), $M=U/a$ is the Mach number of the phase velocity of the disturbance, and A, B, and C are unknown constants to be determined from the boundary conditions. The first term in the square bracket of eq.(5) is the particular solution directly connected to the non-homogeneous term in eq.(4) and the second and the third terms are the homogeneous (general) solutions representing right and left running acoustic waves. In $x>L$, only the right running wave is considered.

The three unknown constants A, B, and C are determined from the following three boundary conditions, where ε is a small positive quantity.

$$u=0 \; at \; x=0 \tag{7}$$
$$u(L-\varepsilon)=u(L+\varepsilon) \tag{8}$$
$$p(L-\varepsilon)=p(L+\varepsilon) \tag{9}$$

The boundary condition (7) is for an ideal case where the gap at the tongue is zero. A more elaborate condition might be required to simulate the present case more precisely. The boundary condition (9) can be reduced to

$$-\frac{v(x)}{b}\bigg|_{x=L-\varepsilon}+\frac{\partial u}{\partial x}\bigg|_{x=L-\varepsilon}=\frac{\partial u}{\partial x}\bigg|_{x=L+\varepsilon} \tag{9'}$$

For the case with only the mass introduction ($f=0$), the constants are determined as follows:

$$A=1-(1-M)e^{-i2\pi Mm}/2,\; B=(1-M)e^{-i2\pi Mm}/2,\; C=1-e^{i2\pi Mm}+(1-M)(e^{i2\pi Mm}-e^{-i2\pi Mm})/2 \tag{10}$$

with $F_{mass}=2\pi m v_0/(bL)$ where v_0 is the amplitude of the normal velocity fluctuation introduced within $0<x<L$, corresponding to the flow rate fluctuation from the stator due to rotor-stator interaction.

Figure 9 shows the amplitude of the velocity disturbance at the volute exit $|u(L)|$, normalized with the amplitude v_0 of the normal velocity introduced within $0<x<L$ for the case of $L/b=22$. This result can be used to predict the amplitude of pressure wave radiation to the volute exit once the amplitude of the velocity fluctuation v_0 due to rotor stator interaction is given. The amplitude takes the maximum value of $L/(2b)$ near $M=1$. This agrees with the experimental results shown in Fig.6, although also the effect of the speed on v_0 is included in the experimental results. It should be noted that the singularity of $1/(1-M^2)$ in eq.(5) is cancelled by a zero embedded in the square bracketed term.

Next, we consider the effect of momentum supply due to rotor-stator interaction. For the case of the momentum supply without mass supply, the first term of equation (9)' disappears. Then the boundary condition results in:

$$A=1+(1-M)e^{-i2\pi Mm}/2M,\; B=-(1-M)e^{-i2\pi Mm}/2M,\; C=1-e^{i2\pi Mm}+(1-M)(e^{i2\pi Mm}-e^{-i2\pi Mm})/2M \tag{11}$$

We evaluate the effects of momentum supply by assuming that the flow is supplied from the stator with an angle of α measured from tangential direction, corresponding to the stator blade angle. The amplitude of the disturbance velocity component normal to the tangential direction is represented by v_0. The fluctuation of momentum supply is evaluated by assuming that the fluctuation is

much smaller than the mean value. Then, it is equated with the mass force in eq.(3). This results in:

$$F_{momentum} = 2\pi m M^2 C_0 \left(\frac{m r_T}{n R r_v}\right) 2\cot\alpha \left(\frac{v_0}{bL}\right) \tag{12}$$

where, r_T is the outer radius of the rotor, r_v is the mean radius of the volute, and $C_0 \equiv \overline{V}_0/U_T$ is the mean radial velocity at the stator outlet normalized with the rotor tip speed. The normalized velocity disturbance at the volute outlet $|u(L)|v_0$, obtained with the values of C_0=0.176, α=13deg, L/b=22, $r_T(nRr_v)$=0.036 corresponding to the experiments, is shown in Fig.10.

Around $M=1$, $|u(L)|/v_0$ takes the maximum value of $C_0\left(\frac{r_T}{nRr_v}\right)\cot\alpha\left(\frac{L}{b}\right)m$. For $M \to \infty$, the envelope tends to $\left(\frac{1}{2\pi}\right)C_0\left(\frac{r_T}{nRr_v}\right)4\cot\alpha\left(\frac{L}{b}\right)$. By comparing the result with those in Fig.9, we find that the contribution of mass introduction is much larger than the effect of momentum introduction.

5.2 Re-examination of the CFD results

First, we consider the pressure wave observed in the volute, shown in Fig.7, as compared with the case of mass introduction. Since it was confirmed that the pattern in the volute propagates with the local flow velocity plus acoustic velocity for the cases of 5,000~10,000rpm, it corresponds to the right running acoustic wave with the amplitude A in eq.(5). At 5,000rpm with $M=1$, the amplitude B of the left running wave becomes zero as shown by eq.(10). At $x=L$, the term corresponding to the right running wave can be expressed as $Ae^{i\left(\frac{2\pi m}{L}U(t-\frac{L}{a})\right)} = Ae^{i\left(\frac{2\pi m}{L}Ut\right)}e^{i(-2\pi mM)}$. This shows that the phase of the disturbance at $x=L$ is delayed behind that at $x=0$ by $2\pi mM$ suggesting that the number of waves in the volute is $m'=mM$. Since the Mach number of the interaction pattern rotation can be evaluated from $M=N/5000$ (N: rpm) we can express $m'=m\times N/5000$. This agrees with the results in Fig.9. Since the amplitudes of the acoustic waves are determined from the boundary conditions (7)-(9), the pressure wave in the volute is caused, not by the accumulation of the disturbance caused by the rotor-stator interaction, but by the interaction of the disturbance with the volute tongue. However, the result of eq.(5) with eq.(10) shows that the amplitude of the particular solution is with the same order of the right running wave. So, it is not clear why only the right running wave is observed in Fig.7.

Figure 11 shows the results at N=3,000rpm. No load flow coefficients at N=3000rpm are ϕ=0.029 for the experiment and ϕ=0.038 for CFD. In addition to the component with *3RN*, the component with *5RN* is found at the volute exit. The amplitude of *5RN* is higher than that of *3RN*. The *5RN* component can be explained from $-2=5\times6-2\times16$, that is, $m=-2$, $n=5$, and $k=-2$. Equation (2) shows that this mode is rotating in the direction opposite to the rotor. The Mach number of the *3RN* component is 0.6, while that of *5RN* component is -1.0. It can be confirmed that $|u(L)|/v_0$ is a function of $|M|$ and does not depend on the direction of the mode rotation. The results in Fig.9 and 10 explain why the amplitude of *5RN* component with $|M|=1$ is larger than that of *3RN* component with $M=0.6$, At higher speed, $|M|$ of *5RN* component becomes much larger than 1 and the component is not detected in the experiment and CFD. The co-existence of *3RN* and *5RN* components is the reason why the propagating nature is not found in Fig.7 at 3,000rpm.

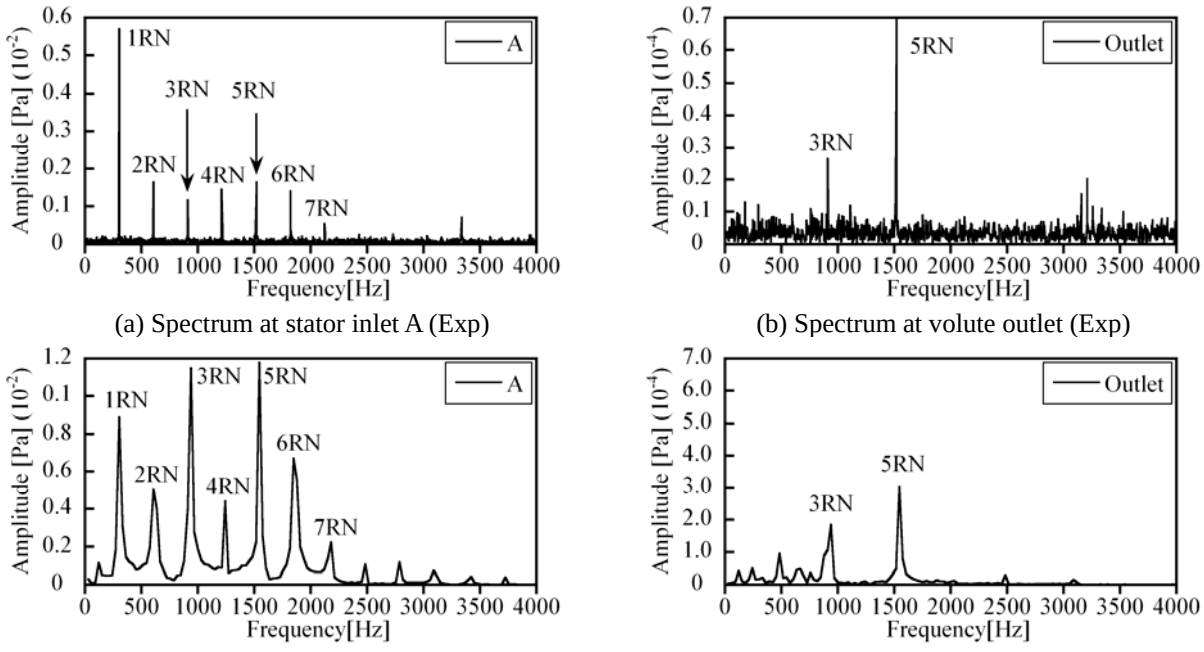

(a) Spectrum at stator inlet A (Exp)

(b) Spectrum at volute outlet (Exp)

(c) Spectrum at stator inlet A (CFD)

(d) Spectrum at volute outlet (CFD)

Fig. 11 Spectra of pressure fluctuation at stator inlet and volute outlet, N=3,000rpm (Exp.: ϕ=0.029, CFD: ϕ=0.038).

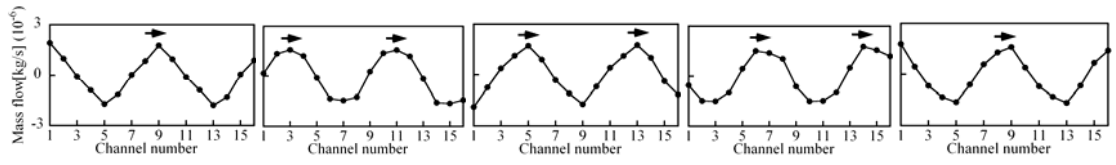

(a) Mass flow at the stator outlet

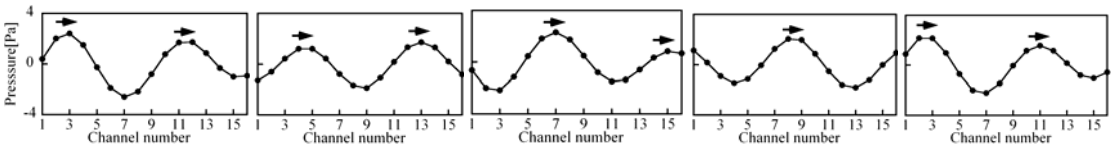

(b) Pressure at the stator outlet

Fig. 12 Mass flow and pressure distribution at the stator outlet, 3000rpm, *3RN* component, Δt=2.58×10^{-4} sec

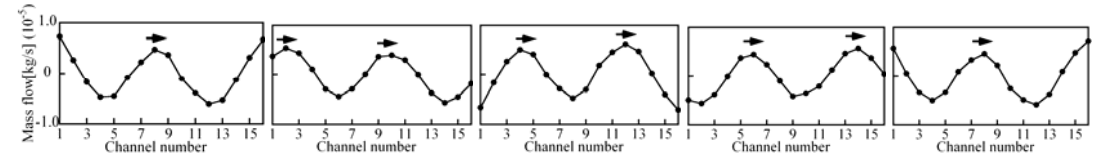

(a) Mass flow at the stator outlet

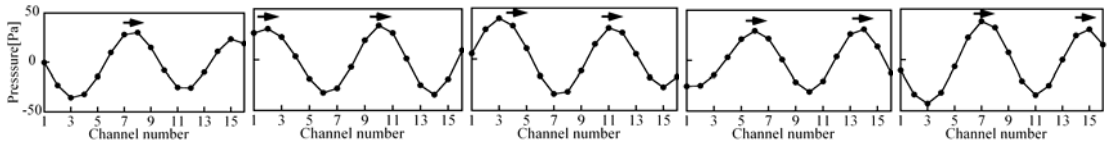

(b) Pressure at the stator outlet

Fig. 13 Mass flow and pressure distribution at the stator outlet, 5000rpm, *3RN* component, Δt=1.56×10^{-4} sec

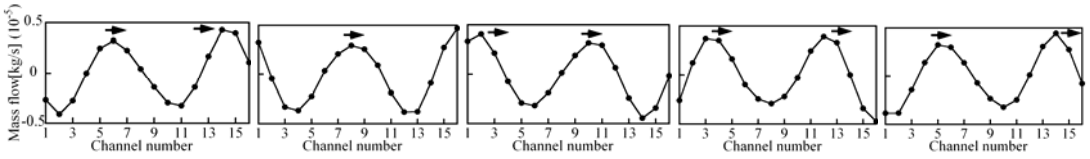

(a) Mass flow at the stator outlet

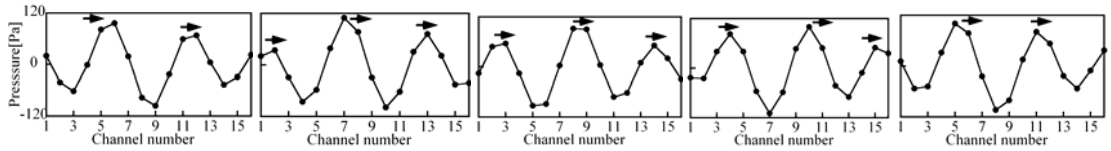

(b) Pressure at the stator outlet

Fig. 14 Mass flow and pressure distribution at the stator outlet, 7000rpm, *3RN* component, Δt=1.13×10^{-4} sec

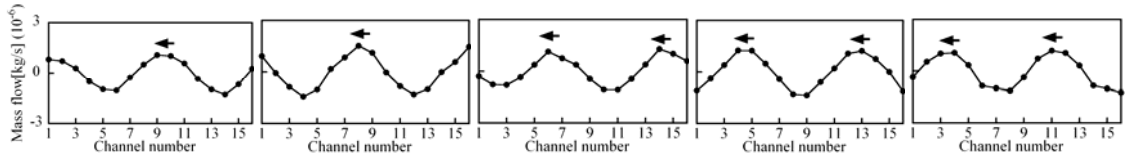

(a) Mass flow at the stator outlet

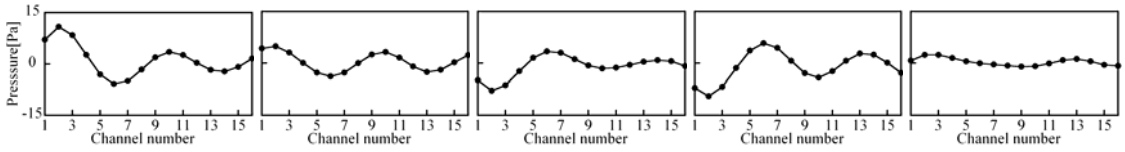

(b) Pressure at the stator outlet

Fig. 15 Mass flow and pressure distribution at the stator outlet, 3000rpm, *5RN* component, Δt=1.29×10^{-4} sec

In order to study the characteristics of each component, CFD results were Fourier analyzed. Figures 12-14 shows the *3RN* components of mass flow and pressure at stator outlet at 3,000, 5,000 and 7,000rpm. The stator channel closest to the tongue is numbered 1, and the channel number increases in the direction of the rotor rotation, as shown in Fig.2. The time step is selected so that one period of *3RN* component corresponds to 4.3 steps. The mass flow has two waves around the periphery for all cases, correspondingly to m=2. The rotational Mach numbers of this mode at the volute mean radius are (*M*=) 0.6, 1.0 and 1.4 for 3,000, 5,000, and 7,000rpm, respectively, rotating in the direction of rotor. Next, we focus on the pressure fluctuation. At 3,000 and 5,000rpm, two waves are rotating at the same speed as the mass flow. So, it corresponds to the particular solution (the first term in the square bracket) of eq.(5). At 7,000rpm, about three pressure waves are rotating in the direction of rotor. Detailed examination

shows that the propagation speed agrees with the sum of fluid velocity and the sound velocity. So, the pressure wave corresponds to the right running acoustic wave (the second term in the square bracket) of eq.(5). Equation (10) shows that the amplitude A of the right running wave is larger at larger M. However, this effect appears more drastically in practical cases shown here.

Figure 15 shows the *5RN* component at 3,000rpm. One period of *5RN* corresponds to 5.16 time step. In the mass flow fluctuation, two periods of wave are rotating in the direction opposite to the rotor rotation, corresponding to $m=-2$. The rotational Mach number of this mode at the mean radius of the volute is evaluated to be one. By putting $M=-1$ in eq.(10), we obtain $A=0$ and $B=1$. So, we should have only left running acoustic wave. However, Fig.15 shows a standing pressure wave with the loops at channel numbers 1, 6, 10, and 14. This suggests that there exists a right running acoustic wave with the same amplitude.

So far we focused on the interaction modes with $m=\pm 2$. However, we also have the modes with -4=2×6-1×16 and 4=6×6-2×16 for $m=nR+kS$. The rotational Mach number is M=0.33 for -4= 2×6-1×16 and M=1 for 4=6×6-2×16 at 5,000rpm. In Fig.5(b), we have a component corresponding to the latter mode with *6RN*, although the level is much lower than the *3RN* component corresponding to 2=3×6-1×16. We do not observe a component with *2RN*, corresponding to -4= 2×6-1×16with M=0.33.

6. Conclusion

Major findings can be summarized as follows:

(1) The phase resonance observed in a pumped storage power plant could be simulated by using a centrifugal compressor for vacuum cleaner.
(2) A large amplitude fluctuation can occur at the volute outlet when the rotational speed of the rotor-stator interaction mode at the volute mean radius agrees with the total of the sound velocity and the fluid velocity.
(3) The amplitude becomes smaller as the rotational Mach number of the mode separates from one.
(4) The phase resonance can occur irrespectively of the direction of the mode rotation.
(5) An acoustic wave occurs in the volute when the Mach number of the interaction mode is larger than 1. When the Mach number is less than 1, the pressure pattern in the volute is fixed to the interaction mode.
(6) A commercial software can simulate the phase resonance reasonably.
(7) A simple one-dimensional theoretical model of phase resonance is proposed. It was clarified that the phase resonance occurs not from the accumulation of the disturbance from each part of interaction mode but from the interaction with the volute. This model can be used to predict the amplitude of pressure wave emitted to the volute exit.
(8) The one-dimensional model simulates the general characteristics (2)-(4) of phase resonance. It was shown that the pressure fluctuation in the volute can be correlated with one of the three components in the model. However, more elaborate boundary conditions may be needed for the model to predict the amplitude of each component more precisely.

Acknowledgments

The authors would like to acknowledge valuable discussions by Dr. Philippe Dupont of Sulzer Corporation and Mr. Keisuke Makikawa of Osaka University for his contributions.

Nomenclature

A, B, C	Unknown constants	S	Number of stator blades
a	Sound velocity [m/s]	t	Time [s]
b	Width of duct [m]	U	Phase velocity of the disturbance [m/s]
C_0	Mean radial velocity at stator outlet normalized with rotor tip speed	U_T	Rotor tip speed [m/s]
		$u(x, t)$	Acoustic velocity in duct [m/s]
D_T	Outlet diameter of rotor [m]	$v(x, t)$	Fluid velocity introduced to duct [m/s]
D_V	Volute mean diameter [m]	v_0	Amplitude of the normal velocity fluctuation [m/s]
f	External mass force [N]	x	Coordinate along duct (volute tongue x=0, volute exit $x=L$) [m]
i	Imaginary unit		
k	Arbitrary integer number	α	Stator outlet blade angle measured from tangential direction [rad]
m,n	Order of harmonics in θ and t		
M	Much number of phase velocity ($=U/a$)	ε	Small positive quantity
N	Rotational speed [rpm]	ϕ	Flow coefficient ($=Q/(U_T D_T^2)$)
p	Pressure [Pa]	θ	Angular location [rad]
p_{in},p_{out}	Inlet total pressure and outlet static pressure [Pa]	ρ	Fluid density [kg/m^3]
Q	Flow rate [m^3/s]	Ω	Angular velocity of rotor [rad/sec]
R	Number of rotor blades	ψ	Pressure coefficient ($=(P_{out}-P_{in})/(0.5\rho U_T^2)$)
r_T	Outer radius of rotor		
r_V	Mean radius of the volute		

References

[1] Ohura, H., Fujii, M., Sugimoto, O., Tanaka, H., and Yamagata, I., 1990, “Vibration of Powerhouse Structure of a Pumped Storage Power Plant,” Proceedings of IAHR Symposium, Belgrade, Yugoslavia.

[2] Den Hartog, J.P., 1929, “Mechanical Vibrations in Penstocks of Hydraulic Turbine Installations,” Transactions of ASME, pp. 101-110.

[3] Chen, Y.N., 1961, “Oscillation of Water Pressure in the Spiral Casing of Storage Pumps, Techn,” Review Sulzer, Research Issue (Turbomachinery), pp. 21-24.
[4] Doerfler, P., 1984, “On the Role of Phase Resonance in Vibration Caused by Blade Passage In Radial Hydraulic Turbomachines,” Proceedings of 12th IAHR Symposium, Stirling.
[5] Makey, E., Cooper, P., Sloteman, D.E., and Gibson, R., “Investigation of Pressure Pulsations Arising from Impeller/Diffuser Interaction in a Large Centrifugal Pump,” Proceedings of Rotating Machinery Conference and Exibition, Nov.10-12, 1993, New Jersey.
[6] Parmakian, J., “Vibration of the Grand Coulee Pump-Discharge Lines,” Transactions of ASME, July, 1954, pp.783-790.
[7] Tyler, J.M., and Sofrin, T.G., 1962, “Axial Flow Compressor Noise Studies,” SAE Trans, Vol.70, pp. 309-332.